CVD Growth Kinetics of HfB_2 Thin Films from the Single-Source Precursor $Hf(BH_4)_4$

Yu Yang,[†,§] Sreenivas Jayaraman,[†,§] Do Young Kim,[‡,§] Gregory S. Girolami,*[,‡,§] and John R. Abelson*[,†,§]

Department of Materials Science and Engineering, University of Illinois at Urbana Champaign, 1304 West Green Street, Urbana, Illinois 61801, Department of Chemistry, University of Illinois at Urbana Champaign, 600 South Mathews Avenue, Urbana, Illinois 61801, and Frederick Seitz Materials Research Laboratory, 104 South Goodwin Avenue, Urbana, Illinois 61801

Received March 6, 2006. Revised Manuscript Received July 15, 2006

Thermal CVD from the single-source precursor $Hf(BH_4)_4$ affords stoichiometric, dense, and hard HfB_2 films; this paper reports the growth kinetics in detail. The decomposition reaction starts at 200 °C; mass spectrometry of the material desorbing from the growth surface reveals that, for steady-state deposition at $P \leq 1 \times 10^{-6}$ Torr, the reaction probability of the precursor is independent of flux and increases with temperature with an apparent activation energy of 0.43 eV. The precursor is less reactive on clean Si and SiO_2 substrates than it is on the HfB_2 growth surface. By analyzing the thickness profile of films grown on high-aspect-ratio trench structures, we find that the growth rate is proportional to $P^{0.3}$ for $1 \times 10^{-4} < P < 1 \times 10^{-2}$ Torr at a substrate temperature of 250 °C. The reaction probability of the precursor decreases from ~1 to 1×10^{-4} as the precursor pressure increases from 1×10^{-6} to 1×10^{-1} Torr. This behavior is consistent with a Langmuirian surface-reaction mechanism. The conformality and the surface morphology of the HfB_2 film are functions of the reaction probability of the precursor molecule. Extremely conformal and smooth coatings on deep trenches (>20:1 aspect ratio) can be obtained at low growth temperatures (≤300 °C) and high precursor pressures (~0.1 Torr) with high growth rates (>200 nm/min).

Introduction

Transition-metal diborides have very useful engineering properties, including high melting point, high hardness, and low electrical resistivity.[1−6] Of the known diborides, HfB_2 is of special interest because it possesses the highest bulk hardness (29 GPa)[7] and its lattice mismatch with GaN is only 1.4%.[8] Recently, we have shown that HfB_2 thin films can be deposited by thermal CVD from the heteroatom-free, single-source precursor $Hf(BH_4)_4$ at low deposition temperatures (≥200 °C).[8] The microstructure and density of the HfB_2 films grown from this precursor change dramatically as a function of growth temperature and pressure, but under lower-temperature and higher-pressure CVD growth conditions, the films are stoichiometric, dense, highly conductive, and highly conformal, making them suitable for electronic applications such as diffusion barriers for copper metallization in ULSI.[8,9] Postannealing of films deposited at 200−300 °C transforms the microstructure from amorphous to nanocrystalline, affording a dramatic increase in the nanoindentation hardness of up to 40 GPa; such films are suitable for use as wear-resistant hard coatings.[9]

In this paper, we report the CVD growth kinetics of HfB_2 films from the precursor $Hf(BH_4)_4$ and describe how the film conformity and film morphology depend on the deposition conditions. The usual method for investigating growth kinetics is to deposit a series of films under a range of deposition conditions and plot the growth rate versus a process parameter such as the substrate temperature or the precursor pressure. Here, we present two elegant methods for obtaining kinetic data as a function of growth temperature and a wide range of pressures. The first method employs temperature-programmed reaction (TPR) spectrometry to determine the temperature dependence of the reaction rate. A line-of-sight mass spectrometer is used to measure the flux of species desorbing from the sample surface. Unlike temperature-programmed desorption, in which the surface is dosed once, in TPR, the surface-desorption rate is measured with the precursor flux on, i.e., the surface reaction is monitored in real time. This technique has been widely used in MBE systems to measure the sticking coefficients of incident molecular beams in order to better control the film

* To whom correspondence should be addressed. E-mail: abelson@mrl.uiuc.edu (J.R.A.).
† Department of Materials Science and Engineering, University of Illinois at Urbana Champaign.
‡ Department of Chemistry, University of Illinois at Urbana Champaign.
§ Frederick Seitz Materials Research Laboratory.

(1) Castaing, J.; Costa, P. *Properties and Uses of Diborides*; Springer-Verlag: Berlin, 1977.
(2) Wuu, D. S.; Lee, M. L.; Lin, T. Y.; Horng, R. H. *Mater. Chem. Phys.* **1996**, *45*, 163−166.
(3) Mitterer, C. *J. Solid State Chem.* **1997**, *133*, 279−291.
(4) Chen, J. S.; Wang, J. L. *J. Electrochem. Soc.* **2000**, *147*, 1940−1944.
(5) Sung, J. W.; Goedde, D. M.; Girolami, G. S.; Abelson, J. R. *J. Appl. Phys.* **2002**, *91*, 3904−3911.
(6) Zagozdzon-Wosik, W.; Darne, C.; Radhakrishnan, D.; Rusakova, I.; van der Heide, P.; Zhang, Z. H.; Bennett, J.; Trombetta, L.; Majhi, P.; Matron, D. *Rev. Adv. Mater. Sci.* **2004**, *8*, 185−194.
(7) Kieffer, R.; Benesovsky, F. *Hartstoffe*; Springer-Verlag: Berlin, 1963.
(8) Jayaraman, S.; Yang, Y.; Kim, D. Y.; Girolami, G. S.; Abelson, J. R. *J. Vac. Sci. Technol., A* **2005**, *23*, 1619−1625.
(9) Jayaraman, S.; Yang, Y.; Gerbi, J. E.; Kim, D. Y.; Chatterjee, A.; Bellon, P.; Girolami, G. S.; Chevalierd, J. P.; Abelson, J. R. *Surf. Coat. Technol.* **2006**, *200*, 6629−6633.

10.1021/cm0605421 CCC: $33.50
Published on Web 09/19/2006

stoichiometry.[10−13] TPR has also been used to study the interaction of gas species with metal or semiconductor surfaces.[14−17] Preliminary TPR results on the deposition of HfB_2 from $Hf(BH_4)_4$ have been presented in a earlier paper;[18] here, we discuss the experimental procedures in detail and describe the reaction probability of the precursor as a function of substrate temperature.

In the second method, films are deposited on high-aspect-ratio macroscopic trenches (25−250 μm wide, 12 mm deep) and the coating profile is analyzed to afford the pressure dependence of the growth rates. The analysis of coating profiles on well-designed structures is a powerful method for acquiring information about growth mechanisms and reaction kinetics.[19−24] Typically, the measured coating profiles are compared with simulations obtained from growth models; the kinetic variables are obtained by fitting the data iteratively. Here, we employ a different approach: by using the continuity equation together with the molecular conductance of a long rectangular slot, we directly calculate the pressure associated with each point of the coating profile, from which we extract the reaction rate as a function of precursor pressure for that substrate temperature. There are several advantages associated with using macroscopic trenches.[21] First, the thickness of the deposited film is negligible compared to the trench opening, so the shape of the trench does not change significantly during film growth, thus greatly simplifying the analysis. Second, the deposition behavior is independent of the absolute dimensions of the structure if they are smaller than the mean free path of the gas. This condition is easily satisfied for low pressure deposition; therefore, the information on reaction kinetics obtained from macroscopic trenches is directly applicable to smaller features. Third, the deposition profile on a macroscopic trench extends to a depth of many millimeters, and by disassembling the trench, a very accurate measurement of thickness and other properties such as film stoichiometry, hardness, electrical conductivity, etc., can be carried out as a function of depth.

By using these two methods, we demonstrate that the growth of HfB_2 follows a first-order Langmuir reaction mechanism and that extremely conformal and smooth coatings can be achieved using low growth temperatures and high precursor pressures. The results show how to obtain a uniformly thick coating of HfB_2 for applications in microelectronics and in MEMS, where there is a need to coat complicated morphologies such as steps, microtubes, narrow trenches, and vias, many of which have high aspect ratios (>20:1).

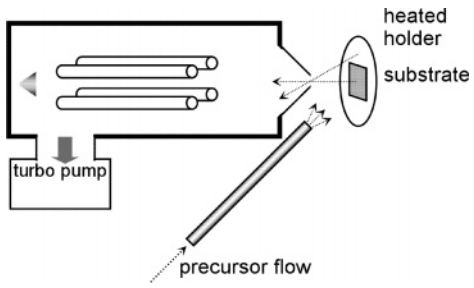

Figure 1. Experimental arrangement for the temperature-programmed reaction studies.

Experimental Section

The experimental setup for the temperature-programmed reaction studies is illustrated in Figure 1. The apparatus is housed in an ion-pumped UHV chamber with a base pressure of 5×10^{-10} Torr. The precursor $Hf(BH_4)_4$ has a very high vapor pressure, 15 Torr at room temperature,[25] and no carrier gas is used. The precursor is air-sensitive and is kept in a stainless steel reservoir equipped with valves such that no air exposure occurs during the filling or use of the reservoir. After passing through the chamber, both unreacted precursor and the reaction product diborane are removed by thermolysis in a high-temperature oven that is part of the exhaust line of the vacuum pumping system. A copious flow of molecular nitrogen is added to the exhaust gas such that the remaining molecular hydrogen is diluted well below its lower flammability limit. The precursor flux, which is controlled by a metering valve, is kept constant during each experimental run. Typically, the metering valve is opened to a set point, at which the absolute molecular throughput (calibrated independently)[18] is 3.2×10^{15} s^{-1}. The maximum precursor flux is limited by the maximum chamber pressure of 1×10^{-5} Torr, the upper limit of the ion pump. The substrates studied in TPR are silicon and silicon covered with 100 nm of thermally grown SiO_2. The silicon substrate is heated by passing direct current through it, and the temperature is controlled by a computer program that modulates the direct current to keep the temperature measured by the thermocouple in accordance with the designated setpoint. Calibration experiments using a pyrometer agree with the thermocouple reading. The sample faces the differentially pumped mass spectrometer (Extrel Max 300) through a 4 mm diameter skimmer cone. The center of the sample, the skimmer entrance, and the orifice of the mass spectrometer ionizer are collinear. The precursor is introduced into the chamber though a 1.6 mm i.d. stainless steel tube, which terminates 5 cm from the sample surface at a 45° angle. In the existing configuration, the skimmer acts only to limit the conductance. The flux entering the mass spectrometer is not limited to that desorbed from the substrate surface, but also includes the flux desorbing from the exposed substrate holder behind the sample (Figure 1) and the flux due to the background pressure inside the chamber. The total signal intensity is therefore expressed as

(10) Evans, K. R.; Kaspi, R.; Ehret, J. E.; Skowronski, M.; Jones, C. R. *J. Vac. Sci. Technol., B* **1995**, *13*, 1820−1823.
(11) Celii, F. G.; Kao, Y. C.; Liu, H. Y. *J. Vac. Sci. Technol., A* **1996**, *14*, 3202−3207.
(12) Kaspi, R.; Loehr, J. P. *Appl. Phys. Lett.* **1997**, *71*, 3537−3539.
(13) Okuyama, H.; Kijima, S.; Sanaka, Y.; Ishibashi, A. *J. Cryst. Growth* **1998**, *193*, 43−49.
(14) Sugiyama, K.; Igari, Y.; Kusunoki, I. *Surf. Sci.* **1993**, *283*, 64−69.
(15) Jones, R. G.; Clifford, C. A. *Phys. Chem. Chem. Phys.* **1999**, *1*, 5223−5228.
(16) Jones, R. G.; Fisher, C. J. *Surf. Sci.* **1999**, *424*, 127−138.
(17) Chan, A. S. Y.; Skegg, M. P.; Jones, R. G. *J. Vac. Sci. Technol., A* **2001**, *19*, 2007−2012.
(18) Jayaraman, S.; Yang, Y.; Kim, D. Y.; Girolami, G. S.; Abelson, J. R. *Journal of Vacuum Science & Technology A* **2005**.
(19) Cheng, L. Y.; McVittie, J. P.; Saraswat, K. C. *Appl. Phys. Lett.* **1991**, *58*, 2147−2149.
(20) Sorita, T.; Shiga, S.; Ikuta, K.; Egashira, Y.; Komiyama, H. *J. Electrochem. Soc.* **1993**, *140*, 2952−2959.
(21) Nuruddin, A.; Doyle, J. R.; Abelson, J. R. *J. Appl. Phys.* **1994**, *76*, 3123−3129.
(22) Soave, R. J.; Ganguli, S.; Gill, W. N.; Shachamdiamand, Y.; Mayer, J. W. *Appl. Phys. Lett.* **1995**, *67*, 3286−3288.
(23) Cale, T. S. *Chem. Eng. Commun.* **1996**, *153*, 261−273.
(24) Tolstopyatov, E. M. *J. Phys. D: Appl. Phys.* **2002**, *35*, 1516−1525.
(25) Hoekstra, H. R.; Katz, J. J. *J. Am. Chem. Soc.* **1949**, *71*, 2488.

$$I = I_{\text{sample}} + I_{\text{holder}} + I_{\text{background}} \quad (1)$$

Because only desorption from sample surface is of interest, the holder and background terms need to be eliminated. $I_{\text{background}}$ is found to be negligible because of the high pumping efficiency. I_{holder} may be on the same order of magnitude as I_{sample} because the exposed area of the substrate holder exceeds that of the sample. As long as no surface reactions occur on the holder, I_{holder} will be a constant. In reality, the temperature of the holder unavoidably rises because of radiative heat transport from the nearby substrate. To keep the holder temperature below the reaction threshold, the experiment must be carried out rapidly. We find that reaction on the holder is negligible over the course of a single ramp to 700 °C if the substrate is heated at a ramp rate of ≥20 °C/s.

In principle, TPR can be used to study all the desorbing species, including the unreacted precursor and surface-reaction products; in practice, the analysis is complicated by the overlap of the various cracking patterns. The mass spectroscopic cracking pattern of Hf-$(BH_4)_4$ contains three groups of peaks: those with m/e ratios of 10−14 are attributed to monoboranes; m/e ratios of 20−28 are attributed to diboranes; and m/e ratios ≥175 contain Hf.[18] In comparison with the spectrum obtained when the substrate is at room temperature, the mass spectrum taken at elevated substrate temperatures is depleted in species with $m/e > 175$ and enriched in species with m/e 10−28; no new peaks are detected. When we scale both spectra so that the peaks at $m/e > 175$ have the same intensity and carry out a subtraction, the resulting spectrum is identical to the cracking pattern of B_2H_6. We conclude that diborane is the only boron-containing product of film deposition under our conditions. The deposited HfB_2 films are stoichiometric by ex situ characterization;[18] therefore, we believe the deposition occurs by means of the following reaction

$$Hf(BH_4)_4 \rightarrow HfB_2 + B_2H_6 + 5H_2 \quad (2)$$

The consumption of precursor as a function of temperature could in theory be followed by measuring either the intensities of the B_2H_6 peaks or the Hf-containing peaks. The former are not good measures of the extent of the reaction, however, because there are background sources of B_2H_6 not related to the deposition process, such as fragmentation of the precursor inside the mass spectrometer. Therefore, in this report, we use the depletion of the peaks due to the precursor as the best measure of the extent of the reaction. Peaks with $m/e \geq 175$ are exclusively from the precursor, and the most intense peak at m/e 208 is used to monitor the precursor concentration.

Film growth on macroscopic trenches was carried out in a companion UHV chamber that is interconnected to the one used for the TPR study. A detailed description of the deposition chamber and growth procedure has been given elsewhere.[18] The macroscopic trench is made with two silicon pieces, between which two tantalum foil strips are placed as spacers (Figure 2). The trench assembly is held onto the substrate holder with two tantalum clamps, which also serve as the electric leads for the resistive heating. A fine (0.005 in. dia.) thermocouple probe was fixed onto the silicon surface by a tantalum clip. As will be shown in the next section, $Hf(BH_4)_4$ reacts with a low probability on the clean Si surface at a low-precursor pressure. To eliminate potential nucleation delays, we evaporated a 20 nm Cr film on the Si pieces before assembly. The silicon pieces act as the trench walls, and their size determines the depth (L) and length (b) of the trench. The thickness of the foil spacer determines the aperture width (d) of the trench. One end of the sandwich structure is sealed with graphite paste to form the bottom of the trench. In our experiments, the trench depths are fixed at 12.5 mm. Foil thicknesses range from 25 to 250 μm; the consequent trench aspect ratios are from 500:1 to 50:1. The choice of aspect ratio depends on the deposition condition chosen; to facilitate analysis (next section), the aspect ratio should be large enough so that deposition ceases at some point above the bottom of the trench. The maximum growth pressure used in this study is 100 mTorr; the gas mean free path is 500 μm at this pressure, which corresponds to molecular flow conditions inside the trench. After a growth run, the trenches are disassembled and the film inside the trench is characterized. To profile the film thickness along the trench depth, cross-sectional scanning electron microscopy images are taken at various places along the middle of the trench wall, as indicated in images b and c of Figure 2.

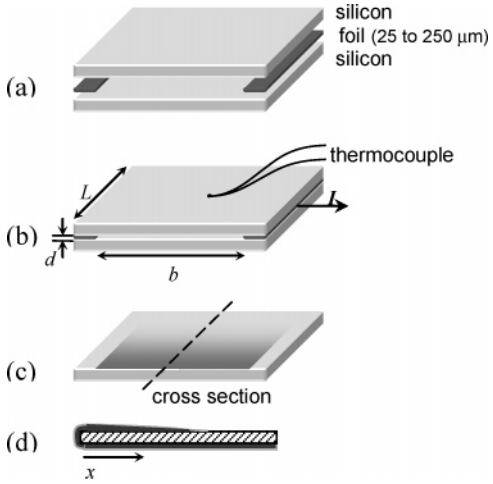

Figure 2. Experimental protocol for film-growth studies in the macroscopic trenches: (a) assembly of the trenches; (b) direct-current heating of the trenches during film growth; (c) disassembly of the trenches, followed by cleaving the side wall to expose a cross-section; (d) typical film-thickness profile in cross-section as determined by SEM.

Results and Discussion

1. Temperature-Programmed Reaction. Consider a steady state in which a precursor flux F impinges on a surface, a reaction occurs at a rate R, and unreacted precursor desorbs at a rate Q. A mass balance for the precursor affords

$$F = Q + R \quad (3)$$

The ratio of the reaction rate to the impingement rate is the surface reaction probability β

$$\beta = \frac{R}{F} \quad (4)$$

$$\frac{Q}{F} = 1 - \beta \quad (5)$$

Because eq 2 is the only reaction we expect from the precursor, the reaction probability is equal to the sticking coefficient. According to eq 1, the mass spectrometer signal is proportional to the desorption rate from the sample surface, plus the contribution of precursor molecules desorbing from the substrate holder

$$I = C_1 Q_{\text{sample}} + I_{\text{holder}} \quad (6)$$

where C_1 is a geometric constant. Assuming a quasi-steady state during the experiment (i.e., the temperature rise is small during the data-acquisition time of the mass spectrometer),

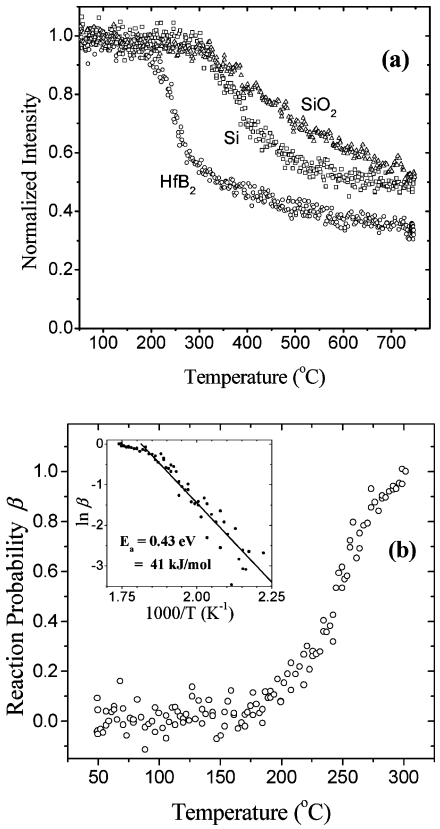

Figure 3. (a) Plots of intensity of the Hf-containing $m/e = 208$ peak vs temperature, as determined from temperature-programmed reaction experiments in which 1×10^{-7} to 1×10^{-6} Torr of the precursor $Hf(BH_4)_4$ was passed over Si, SiO_2, and HfB_2 surfaces. (b) Temperature dependence of the $Hf(BH_4)_4$ reaction probability on a HfB_2 surface; insert shows the same data as an Arrhenius plot. Data taken from ref 8.

then according to eq 5, I is related to the reaction probability as

$$I = C_1F(1 - \beta) + I_{\text{holder}} \tag{7}$$

We have applied this analysis to the deposition of HfB_2 films from the single-source precursor $Hf(BH_4)_4$. The reaction is followed by temperature-programmed reaction spectroscopy, in which the rate of precursor desorption is monitored at a constant precursor flux as the surface temperature is ramped linearly. In Figure 3a, the intensity of the precursor peak with m/e 208 measured during a TPR experiment is plotted versus substrate temperature. All of the data are normalized to the intensity seen in the low-temperature limit (50 °C), where no reaction occurs. The open circles are data obtained from a substrate already coated with a HfB_2 film. Three regimes are clearly identified in this plot: constant intensity at $T < 200$ °C, a decrease from 200 °C $\leq T \leq$ 350 °C, and almost constant intensity at $T > 350$ °C. In the first regime, the substrate temperature is below the reaction threshold, identified as 200 °C from the plot, and the precursor desorbs with high efficiency from the surface. In the second regime, the surface-reaction rate increases with temperature and less and less precursor is seen because it is being consumed by the surface reaction. When the reaction rate becomes comparable to the incoming flux F, the growth should become flux limited; this is the third regime, where the reaction probability β saturates at a maximum value. In the following analysis, we will assume that reaction probability in the third regime has saturated, i.e., $\beta = 1$, for purposes of extracting the apparent activation energy. According to eq 7, in this high-temperature regime, I is equal to I_{holder}, which is the signal due to unreacted precursor molecules desorbing from the substrate holder. In Figure 3a, the signal due to intact precursor molecules actually drops slightly because an increasing fraction of them decompose on the holder as it heats above 200 °C late in the experimental run. In fact, when we carry out the TPR experiment with a slower ramp rate, the holder is heated more severely and consumes more precursor, and I_{holder} drops much more significantly. Here. the ramp rate is fast enough that we can consider I_{holder} to be a nearly constant; the reaction probability of the precursor can then be calculated from eq 7

$$\beta = 1 - \frac{I - I_{\text{holder}}}{C_1F} = 1 - \frac{I - I_{\text{holder}}}{I_0 - I_{\text{holder}}} \tag{8}$$

where I_0 is the constant intensity seen at substrate temperatures below 200 °C, where no surface reaction occurs. A plot of β versus temperature is given in Figure 3b. As shown in the insert of Figure 3b, $\ln(\beta)$ is linearly dependent on $1/T$ below 270 °C, indicating an Arrhenius dependence with an apparent activation energy of 0.43 eV (41 kJ/mol). The relatively low activation energy is consistent with the low reaction-onset temperature of this precursor. The reaction rate is thus

$$R \propto F \exp\left(\frac{-0.43\ \text{eV}}{kT}\right) \tag{9}$$

The TPR experiment on a HfB_2 surface has been repeated with a range of fluxes that correspond to precursor pressures of 1×10^{-7} to 1×10^{-6} Torr. By normalizing to I_0, the I versus T plots obtained in this pressure range are essentially identical to those shown in Figure 3a; this result is consistent with the functional form of eq 9, which assumes that the reaction probability (R/F) is independent of flux. Under these low-pressure conditions, we expect the film growth rate to be linearly dependent on P, the precursor partial pressure.

Figure 3a also shows the results of TPR experiments on clean silicon and SiO_2 substrates. Note that a clean surface persists for only one TPR run, after which it will be coated with a thin HfB_2 film. The initiation of the deposition reaction, as determined by the onset of precursor consumption, is ~100 °C higher on the clean Si and SiO_2 substrates, indicating the presence of a nucleation barrier. The existence of this barrier is further confirmed by growth experiments conducted at constant temperature. At low precursor pressures ($<1 \times 10^{-6}$ Torr), no film grows on clean silicon and SiO_2 substrates at $200 < T < 300$ °C for at least 30 min; in contrast, growth does occur on HfB_2 under these conditions. Note that this behavior could form the basis of a surface-selective growth method. To achieve film growth on Si or SiO_2 at low temperatures, the precursor flux must be increased substantially ($>1 \times 10^{-4}$ Torr) until nucleation occurs, or the film must be grown on a previously deposited HfB_2 film or other surface that promotes nucleation. This growth barrier is not the thermodynamic barrier described

by classical capillary theory: the growth temperature is so low in comparison with the melting temperature of HfB_2 (3250 °C) that the critical nucleus size is unphysical, smaller than one atom.[26] Rather, the growth is limited by the barrier for the reaction between the precursor and the chemical structures — the terminal groups, the dangling bonds, and the defects — present on the initial surface. With respect to the precursor $Hf(BH_4)_4$, the growth-onset temperature indicates that HfB_2 is a more reactive surface than Si and SiO_2. Previous studies of HfB_2 surfaces suggest that the film surface contains excess Hf,[27,28] and we speculate that the presence of the transition metal facilitates dissociative chemisorption of the precursor. In fact, the growth on evaporated transition-metal films of Ti and Cr is very similar to the growth on HfB_2. In real-time spectroscopic ellipsometry measurements, we do not observe any nucleation delay on these metallic surfaces under low-temperature and low-pressure growth conditions, for which the growth on Si or SiO_2 is strongly nucleation-limited.

On the three surfaces (HfB_2, Si, and SiO_2), the reaction rates have different temperature dependences, as indicated by the different slopes in Figure 3a. On the HfB_2 surface, the reaction rate is governed by the growth kinetics below 300 °C and is flux-limited above this temperature. In contrast, on silicon and SiO_2 surfaces, the reaction rate is governed by a convolution of a slow reaction rate on the original substrate and a faster rate on the HfB_2 surface, whose coverage increases from zero to one over the course of the experiment. Because the film and the exposed substrate have different reactivity toward the precursor, the consumption of the precursor can be expressed as

$$I_0 - I = FC_1[\beta_f\theta_f + \beta_s(1 - \theta_f)] \qquad (10)$$

where θ_f is the HfB_2 film coverage and the subscripts f and s denote film and substrate, respectively. A smaller precursor-consumption rate indicates a smaller surface-reaction probability for the $Hf(BH_4)_4$ molecule, thus $\beta_{SiO2} < \beta_{Si} < \beta_f$ is inferred from Figure 4a. A lower substrate surface reactivity leads to a smaller film-nucleation rate and a longer growth-incubation time; in addition, the film is highly rough during its initial (precoalescence) growth stage. A detailed real-time spectroscopic ellipsometry study confirms this expectation: the HfB_2 films nucleate more slowly and are rougher when grown on SiO_2 substrates than when they are grown on Si substrates.[29]

2. Growth on Macroscopic Trenches. We have independently measured the growth kinetics for the deposition of HfB_2 from the single-source precursor $Hf(BH_4)_4$ using macroscopic trenches. After the growth run, the trenches are disassembled and the growth profiles are easily measured. A typical thickness profile of a HfB_2 film grown in a macroscopic trench is shown in Figure 4a. For this experiment, the trench width was 65 μm, the precursor pressure was 10 mTorr, and the substrate temperature was 250 °C. Several cross-sectional SEM images taken from different positions of this trench are shown in Figure 5. The thickness profile is plotted as a function of x/d, where x is the depth in the trench (measured from the trench opening) and d is the width of the trench opening, as defined in Figure 2b. The aspect ratio of this trench is 192:1; under the growth conditions given above, the film grows to a depth of $x/d = 110$. Because the opening of the trench is the only source of precursor, there is a net flux of precursor from the opening toward the bottom of the trench; the flux decreases with depth because of film deposition on the walls.

To derive quantitative information from the profile, we solve the steady-state continuity equation as follows. The

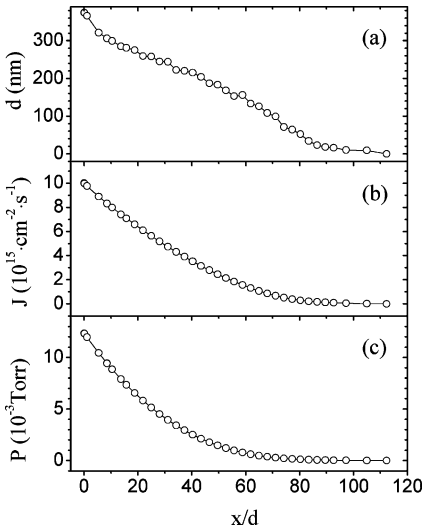

Figure 4. For a HfB_2 film deposited at 250 °C and 10 mTorr precursor pressure in a 65 μm width macroscopic trench: (a) experimental thickness profile; (b) flux profile calculated from eq 11; (c) pressure profile calculated from eq 15.

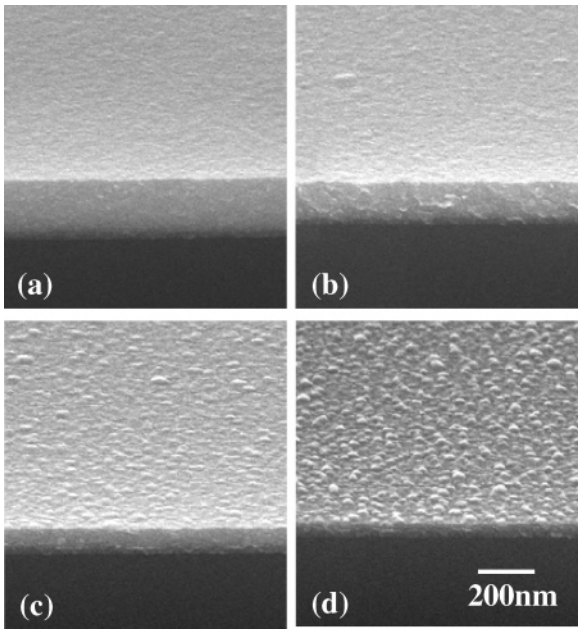

Figure 5. Scanning electron micrographs showing HfB_2 film thickness and morphology within the macroscopic trench of width 65 μm at x/d values of (a) 45, (b) 60, (c) 75, and (d) 90. The film was grown at 250 °C and 10 mTorr.

(26) Thompson, C. V.; Carel, R. *Mater. Sci. Eng., B* **1995**, *32*, 211−219.
(27) Perkins, C. L.; Singh, R.; Trenary, M.; Tanaka, T.; Paderno, Y. *Surf. Sci.* **2001**, *470*, 215−225.
(28) Hayami, W.; Souda, R.; Aizawa, T.; Tanaka, T. *Surf. Sci.* **1998**, *415*, 433−437.
(29) Yang, Y.; Jayaraman, S.; Kim, D. Y.; Girolami, G. S.; Abelson, J. R. *J. Vac. Sci. Technol., A*, submitted.

flux passing through any cross-section of the trench equals the total quantity of material deposited downstream of that position; therefore, the time average flux can be calculated by integrating the thickness profile of the film

$$J(x)\tau bd = 2\int_x^\infty bt(x)\rho dx \tag{11}$$

where $J(x)$ is the net flux at depth x; b is the length of the slot that defines the trench opening; ρ is the atomic density of Hf in the film (because each precursor molecule transports one Hf atom); $t(x)$ is the thickness of the film at depth x; and τ is the duration of growth. The integral expression assumes that the width of the trench opening d is negligible compared to the slot length of the trench opening b, such that the narrow side walls can be neglected. The flux is related to the pressure P according to Fick's law of diffusion

$$J(x) = -\frac{D}{kT}\frac{dP}{dx} \tag{12}$$

where D is the diffusivity. In the molecular-flow regime, the usual definition of diffusivity is not applicable because the transport behavior is determined by wall collisions, i.e., by the gas conductance C. For structures with a uniform cross-section along their length, the unit conductance is a constant and is represented by an effective diffusivity

$$D = CL/A \tag{13}$$

where L and A are the length and cross-sectional area of the conductor. The conductance of a trench in units of liters per second, as derived from the analysis of a rectangular duct with infinite width,[30] is

$$C = 9700\,\frac{bd^2}{L}\left(\frac{T}{M}\right)^{1/2} \tag{14}$$

where M is the molecular weight of the gas molecule. By integrating eq 12, we can calculate the pressure from the thickness profile alone. By properly selecting the trench aspect ratio and deposition conditions, we can ensure that the coating does not extend to the bottom of the trench, so that the boundary condition is $P = 0$ at infinite depth in the trench. The pressure is expressed as

$$P(x) = \frac{kT}{9700\,d\left(\frac{T}{M}\right)^{1/2}}\int_x^\infty J(x)dx \tag{15}$$

We assume that the film has 70% of the theoretical bulk density; we determined this value in separate growth experiments on planar substrates across a wide range of pressures at these temperatures.[18] The flux and pressure profiles are presented in parts b and c of Figure 4. At the trench opening, the precursor pressure calculated from the thickness profile is ~20% larger than the precursor pressure in the growth chamber. This overestimate results largely from the fact that the conductance at the opening of the trench, as with any cross-section, is significantly larger than the conductance within the trench.[31] Therefore, the pressure calculated using eq 15 is underestimated. However, there is no explicit analytic expression available to describe the opening of a tube. In addition, the precursor is injected at room temperature and must heat up to the growth temperature as the result of one or more collisions with the trench wall; however, this effect is expected to be minor compared to the underestimate of the conductance near the trench opening.

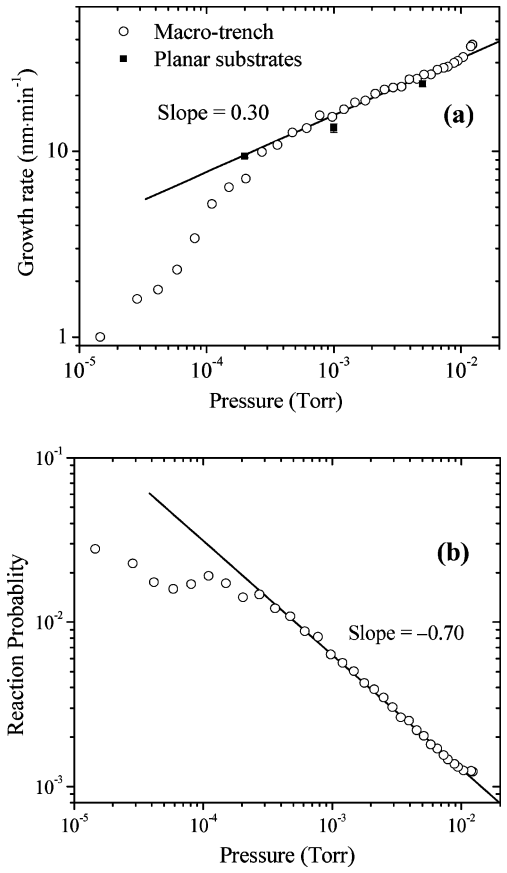

Figure 6. Growth kinetics obtained from the macroscopic trench experiment at 250 °C: (a) growth rate vs pressure; (b) reaction probability vs pressure.

Figure 6a shows the HfB_2 film growth rate vs the precursor pressure on a log−log scale. Also shown are growth rates obtained from separate depositions on planar substrates. The data obtained from the macroscopic trenches are in excellent agreement with those measured on planar substrates, indicating that the present analysis is valid. In the precursor pressure range of 1×10^{-4} to 1×10^{-2} Torr, the reaction rate is proportional to $P^{0.3}$. The growth rate at $P < 1 \times 10^{-4}$ Torr shows a stronger (roughly linear) dependence on pressure; these data are derived from the tail end of the profile, where the analysis has lower accuracy because the film thickness is close to the SEM resolution of a few nanometers.

The surface reaction rate R (per precursor molecule per unit area) equals the film growth rate multiplied by the Hf atomic density. Thus, the reaction probability β at each pressure can be calculated from eq 4; Figure 6b shows that β is proportional to $P^{-0.7}$ in the 1×10^{-4} to 1×10^{-2} Torr pressure range at this substrate temperature (250 °C).

(30) Ohring, M. *Materials Science of Thin Films*, 2nd ed.; Academic Press: New York, 2001.

(31) O'Hanlon, J. F. *A User's Guide to Vacuum Technology*, 2nd ed.; John Wiley & Sons: New York, 1980.

3. Reaction Mechanism. The experimental results discussed above indicate that the HfB_2 growth rate has a varying dependence on precursor pressure, depending linearly on P at low pressures ($<1 \times 10^{-6}$ Torr) and as $\sim P^{0.3}$ at higher pressures (1×10^{-4} to 1×10^{-2} Torr). The change of reaction order with precursor pressure is a well-known feature of Langmuir adsorption processes in which the net reaction rate becomes limited by the surface coverage of adsorbed precursor molecules. The first-order Langmuir mechanism has the following reaction-rate expression

$$R = k_s S_0 \frac{KP}{1 + KP} \tag{16}$$

where S_0 is the surface site density, P is the precursor pressure, k_s is the surface reaction rate constant, and K is the adsorption equilibrium constant. The ratio $KP/(1 + KP)$ represents the fractional steady-state surface coverage predicted by the Langmuir isotherm. In this reaction-rate expression, the reaction order is 1 at low pressure ($KP \ll 1$) and 0 at high pressure ($KP \gg 1$). At low pressures, the impingement rate is smaller than the surface reaction rate and most of the surface sites are available for adsorption and further reaction. At high pressures, the impingement rate is much higher than the reaction rate and the surface sites become blocked by adsorbed molecules that have not reacted completely. Arriving molecules that cannot find an available surface site will desorb without reaction. Our experimental results qualitatively follow the first-order Langmuir mechanism.

However, it is unexpected that the growth rate should obey $P^{0.3}$ over 2 orders of magnitude (Figure 6); the Langmuir mechanism predicts that growth rate should reach an asymptote at higher pressures. One possible explanation involves additional site-blocking by reaction products. Raupp et al.[32] simulated the profile of SiO_2 deposited by thermal CVD from TEOS inside a 3.5:1 aspect ratio trench; they determined that the growth rate was smaller than that predicted by a Langmuir mechanism similar to eq 16. They proposed that film growth can be inhibited by reaction byproducts, which can readsorb and occupy reaction sites, thus reducing the surface coverage of the precursor molecule and decreasing the overall reaction rate. Byproduct inhibition would reduce the growth rate inside any high-aspect-ratio recessed structure, because the limited conductance of the opening will cause the byproduct to accumulate inside the recess. However, we have observed that the growth rate on planar substrates, which should be essentially unaffected by byproduct inhibition, are very similar to those measured in the macroscopic trenches (Figure 4a); hence, we exclude this possibility as an explanation for the deviation of the HfB_2 film growth kinetics from the ideal Langmuirian model.

For an ideal Langmuir process, the transition between the flux-limited and reaction-limited regimes should spans about 2 orders of magnitude in pressure, i.e., $0.1/K < P < 10/K$, as suggested by eq 16. We propose that the transition from the flux-limited to the reaction-limited regime in our system occurs over a wider pressure range because the amorphous HfB_2 film has a distribution of surface structures, adsorption energies, and reaction barriers. Within a certain pressure range of the transition regime, the adsorption behavior for such a surface can be fitted to a power law equation

$$\theta = \alpha_F P^{C_F}. \tag{17}$$

This equation, usually called the Freundlich isotherm, is purely empirical.[33] Therefore, the 0.3 order dependence of the HfB_2 growth rate on pressure at 1×10^{-4} to 1×10^{-2} Torr is characteristic only of this transition regime, and a continued increase in the precursor pressure should eventually lead to growth-rate saturation and zero-order kinetics.

4. Conformal Coverage and Surface Morphology. A thin-film growth process will be conformal on a nonplanar substrate when the adsorbed precursor can diffuse on the film surface, or when the precursor has a high probability of re-emission into the gas phase (i.e., a low sticking coefficient). Which of these mechanisms is dominant can be determined by measuring the coating profile on an overhanging test structure.[19] Most often, the surface diffusion length is less than the feature size of the structures that need to be coated, so that the contribution of surface diffusion to the conformal coverage is small; this will certainly be true in the macrotrench that is $\sim$1 cm deep. The re-emission mechanism depends on the aspect ratio (shape) of the structure but not on its absolute size, provided that the distance between nearby surfaces is less than the mean free path for gas-phase collisions, i.e., the precursor transport is dominated by molecular flow. (Conformal coverage is also possible in the case of viscous or transition flow, but the typical case in microelectronics involves very small features and a low-pressure deposition process, i.e., molecular flow conditions.) Therefore, the most general method for obtaining a uniform coating on a complicated surface topography is to select growth conditions that ensure a low precursor sticking coefficient.[19]

In our process, we assume that the net sticking coefficient of the precursor is equal to the reaction probability R defined by eq 4, because the precursor itself is the only volatile MB_xH_y species known. (If an incoming growth species can recombine with a surface-bound species to produce a different volatile molecule, as in plasma-enhanced CVD, then the conformal coverage will depend on the total surface reaction probability β, which is the sum of the sticking (film growth) probability R and the surface-recombination probability γ.[21]) For the conformal coverage on structures with arbitrary topographies to be accurately predicted, modeling and simulation methods must be used.[24,34−39] The case of a deep rectangular trench has been extensively discussed because

(32) Raupp, G. B.; Shemansky, F. A.; Cale, T. S. *J. Vac. Sci. Technol., B* **1992**, *10*, 2422−2430.
(33) Masel, R. I. *Principles of Adsorption and Reaction on Solid Surfaces*; Wiley: New York, 1996.
(34) Rey, J. C.; Chen, L. Y.; McVittie, J. P.; Saraswat, K. C. *J. Vac. Sci. Technol., A* **1991**, *9*, 1083−1087.
(35) Wulu, H. C.; Saraswat, K. C.; McVittie, J. P. *J. Electrochem. Soc.* **1991**, *138*, 1831−1840.
(36) Akiyama, Y.; Matsumura, S.; Imaishi, N. *Jpn. J. Appl. Phys.* **1995**, *34*, 6171−6177.
(37) Rodgers, S. T.; Jensen, K. F. *J. Appl. Phys.* **1998**, *83*, 524−530.
(38) Gobbert, M. K.; Merchant, T. P.; Borucki, L. J.; Cale, T. S. *J. Electrochem. Soc.* **1997**, *144*, 3945−3951.

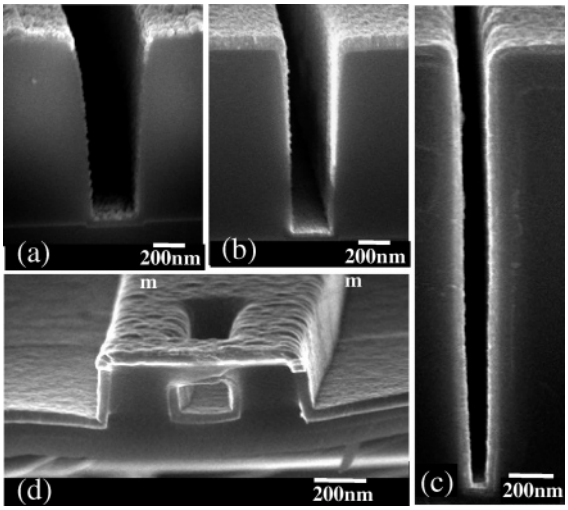

Figure 7. Scanning electron micrographs of HfB_2 films grown on recessed structures at (a) 300 °C and 1×10^{-6} Torr; (b) 225 °C and 1×10^{-6} Torr; (c) 200 °C and 8×10^{-2} Torr; and (d) 300 °C and 1×10^{-1} Torr.

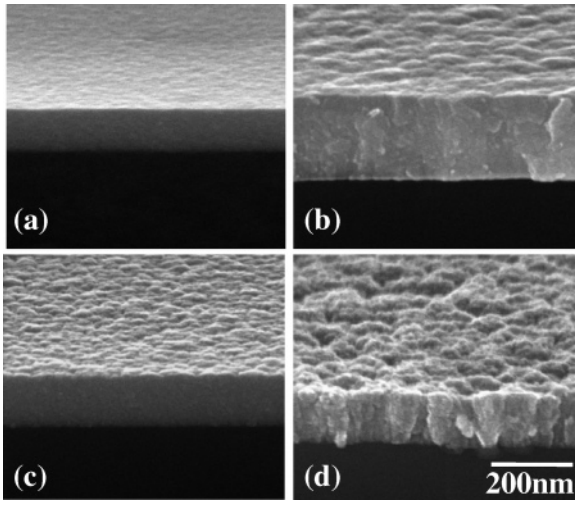

Figure 8. Scanning electron macrographs of HfB_2 films grown on planar substrates at 275 °C and precursor pressures of: (a) 5×10^{-3} Torr; (b) 1×10^{-3} Torr; (c) 1×10^{-4} Torr; and (d) 1×10^{-5} Torr.

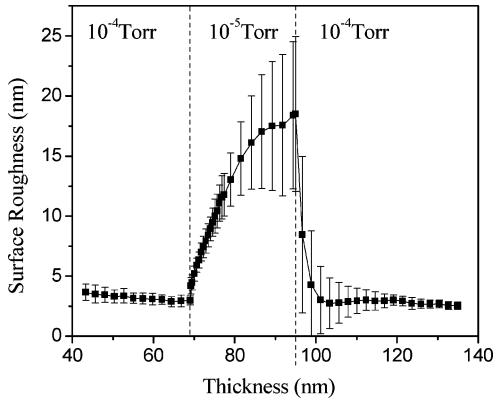

Figure 9. Surface roughness evolution of a HfB_2 film grown at 275 °C with the precursor pressure modulated between 1×10^{-4} and 1×10^{-5} Torr, measured by in situ ellipsometry spectroscopy.

of its relevance in microelectronics manufacturing; here, we restrict our attention to this well-understood simple structure and discuss the relationship between the reaction probability R and the degree of conformal coverage.

In the low-pressure regime ($P < 1 \times 10^{-6}$ Torr), the reaction probability is a function only of the substrate temperature T (Figure 3b). At temperatures above 300 °C, the reaction probability is close to unity; consequently, the coverage is nonconformal and the microstructure is columnar with high roughness and low atomic density (Figure 7a), similar to PVD conditions in the absence of any surface diffusion.[40] The conformality can be improved somewhat by decreasing the growth temperature. For example, at 225 °C (Figure 7b), the reaction probability is 0.25 and the conformality is improved but is still insufficient to coat a 7:1 aspect-ratio trench uniformly.

In the high-pressure regime ($P > 1 \times 10^{-4}$ Torr), the reaction probability, which is proportional to $P^{-0.7}$ at 250 °C (Figure 6b), can be efficiently decreased by raising the precursor pressure. In the macrotrench experiment using a 1×10^{-2} Torr pressure, the coating extends to an aspect ratio greater than 100:1. For a trench with modest aspect ratio such as the one shown in Figure 7c (depth:width = 13:1), the step coverage is essentially 100%. Note that the vapor pressure of $Hf(BH_4)_4$ is 15 Torr at room temperature. Taking this as the maximum experimental pressure, we can further decrease the reaction probability, in principle, by 2 orders of magnitude assuming that the $P^{-0.7}$ dependence continues to hold true; this provides a means to achieve conformal coverage on much higher aspect ratio structures. In the high-pressure regime, the growth rate is insensitive to pressure because the surface is always saturated with adsorbed precursor molecules. However, the reaction rate constant k_s has an Arrhenius temperature dependence. Therefore, a slightly higher temperature can be used in conjunction with a high precursor pressure to achieve simultaneously a high growth rate and good conformal coverage. For example, in Figure 7d, a precursor pressure of 0.1 Torr and a temperature of 300 °C yield a highly conformal film at a growth rate of 200 nm/min.

A striking phenomenon we observed in the CVD growth of HfB_2 is the strong dependence of film surface morphology on precursor pressure. Figure 8 shows four films grown to similar thicknesses at 275 °C under different precursor pressures. At 1×10^{-5} Torr, the film is essentially columnar (Figure 8d). As the pressure increases to 5×10^{-3} Torr, the columnar structure disappears and the surface becomes much smoother (Figure 8a−c). Similar trends can also be observed in Figure 5, where the films are rougher at positions deeper in the macroscopic trench (larger x/d). This is another example demonstrating the elegance of the macroscopic trench method: the dependence of film properties on the growth pressure can be determined in just one growth run. The pressures corresponding to the positions shown in Figures 5a−d are 2.0, 0.7, 0.2, and 0.04 mTorr, respectively.

We also used in situ spectroscopic ellipsometry to study the evolution of surface roughness with precursor pressure in a single growth run. As shown in Figure 9, when the precursor pressure was abruptly decreased from 1×10^{-4} to 1×10^{-5} Torr, the surface roughness increased from 3 nm to more than 10 nm; these pressures correspond approx-

(39) Islamraja, M. M.; Cappelli, M. A.; McVittie, J. P.; Saraswat, K. C. *J. Appl. Phys.* **1991**, *70*, 7137−7140.
(40) Thornton, J. A. *J. Vac. Sci. Technol., A* **1986**, *4*, 3059−3065.

imately to the surfaces shown in images c and d of Figure 8, respectively. However, when the pressure was abruptly restored to 1×10^{-4} Torr, the roughness decreased to near its original value. This result, similar to that from our studies of amorphous silicon growth on intentionally rough substrates,[41] demonstrates that surface roughness is a dynamic quantity; it results from the competition between instabilities that promote roughness and mechanisms that promote smoothing.[42] The leading instability is microscopic self-shadowing, which involves a higher growth rate on surface protrusions than in depressions.[40] The leading smoothing mechanisms are surface diffusion and low reaction probability. Note that the roughness reported here is the thickness of an effective medium layer composed of 50% film and 50% voids. This approximation gives a reliable roughness value for the smooth films but, as indicated by the large error bars, becomes imprecise for the rough surfaces.[43]

It is interesting to consider which mechanism is responsible for the rapid self-smoothing shown in Figure 9. It is tempting to assume that surface diffusion cannot be responsible because the homologous temperature $T/T_m = 0.15$ is so low, and because the substrate temperature is not varied during the experiment. However, if diffusion were mediated by a layer of adsorbed precursor molecules and/or reaction intermediates, and if the adsorbed populations varied with precursor pressure as described by eqs 16 and 17, then surface diffusion rates could be changing significantly with pressure. Surface diffusion is thought to be an important smoothing mechanism in the deposition of amorphous silicon at low temperatures, which also involves adsorbed precursors.[43,44] Thus we cannot rule out the possibility that surface diffusion contributes to the rapid self-smoothing as the pressure is raised.

Re-emission of the adsorbed species can also suppress growth instabilities. Depressions on the surface are qualitatively similar to microscopic trenches, and a low surface-reaction probability leads to conformal coverage and eventual filling of such structures. We have shown that the sticking coefficient of the precursor $Hf(BH_4)_4$ is a strong function of the pressure (Figures 3b and 6b). Zhao et al.[45] used computer modeling to show that the surface morphology changes from columnar to self-affine, and the rate of surface roughening becomes smaller, as the sticking coefficient decreases. Our results are consistent with this model study, and we conclude that a low reaction probability is likely to be the principal factor that leads to very flat HfB_2 surfaces by CVD.

Conclusions

For the chemical vapor deposition of HfB_2 thin films from the single-source precursor $Hf(BH_4)_4$, the growth rate is proportional to precursor pressure in the low-pressure regime ($<1 \times 10^{-6}$ Torr) and is proportional to $\sim P^{0.3}$ in a higher-pressure regime ($1 \times 10^{-4} < P < 1 \times 10^{-2}$ Torr). The surface-reaction probability is very low on clean silicon and SiO_2 substrates, but nucleation can be initiated at high ($\sim 1 \times 10^{-4}$ Torr) precursor pressures. On HfB_2 surfaces, the surface-reaction probability falls from ~ 1 to $< 1 \times 10^{-4}$ between the low- and high-pressure limits. The growth behavior qualitatively follows a Langmuir adsorption mechanism. The nonzero reaction order in the high-pressure regime probably reflects inhomogeneities in the surface. The conformality as well as the morphology of the HfB_2 film is strongly dependent on the reaction probability of the precursor molecule: lower reaction probabilities afford smooth, dense films with excellent step coverages. Extremely conformal coatings on deep trenches (>20:1 depth:width) can be attained in the high-pressure regime, and high growth rates (>200 nm/min) can be sustained using moderate substrate temperatures (~300 °C). These attributes make the CVD growth of HfB_2 and related systems very attractive for technological applications.

Acknowledgment. The authors are grateful to the National Science Foundation for support of this research under grants CHE 00-76061, DMR 03-54060, and DMR 04-20768. Compositional and structural analyses of the films were carried out in the Center for Microanalysis of Materials, University of Illinois, which is supported by the U.S. Department of Energy under Grant DOE DEFG02-91ER45439.

CM0605421

(41) Sperling, B. A.; Abelson, J. R. *Appl. Phys. Lett.* **2004**, *85*, 3456−3458.
(42) Cahill, D. G. *J. Vac. Sci. Technol., A* **2003**, *21*, S110−S116.
(43) Gerbi, J. E.; Abelson, J. R. *J. Appl. Phys.* **2001**, *89*, 1463−1469.
(44) Bray, K. R.; Parsons, G. N. *Phys. Rev. B* **2002**, *65*, 035311.
(45) Zhao, Y. P.; Drotar, J. T.; Wang, G. C.; Lu, T. M. *Phys. Rev. Lett.* **2001**, *8713*, 136102.